

On the Pulse Intensity Modulation of PSR B0823+26

N. J. Young,^{1*} B. W. Stappers,¹ P. Weltevrede,¹ A. G. Lyne¹ and M. Kramer^{2,1}

¹*Jodrell Bank Centre for Astrophysics, The University of Manchester, Alan-Turing Building, Manchester M13 9PL, United Kingdom*

²*Max-Planck-Institut für Radioastronomie, Auf dem Hügel 69, 53121 Bonn, Germany*

24 August 2012

ABSTRACT

We investigate the radio emission behaviour of PSR B0823+26, a pulsar which is known to undergo pulse nulling, using an 153-d intensive sequence of observations. The pulsar is found to exhibit both short (\sim min) and unusually long-term (\sim hours or more) nulls, which not only suggest that the source possesses a distribution of nulling timescales, but that it may also provide a link between conventional nulling pulsars and longer-term intermittent pulsars. Despite seeing evidence for periodicities in the pulsar radio emission, we are uncertain whether they are intrinsic to the source, due to the influence of observation sampling on the periodicity analysis performed. Remarkably, we find evidence to suggest that the pulsar may undergo pre-ignition periods of ‘emission flickering’, that is rapid changes between radio-on (active) and -off (null) emission states, before transitioning to a steady radio-emitting phase. We find no direct evidence to indicate that the object exhibits any change in spin-down rate between its radio-on and -off emission modes. We do, however, place an upper limit on this variation to be $\lesssim 6\%$ from simulations. This indicates that emission cessation in pulsars does not necessarily lead to large changes in spin-down rate. Moreover, we show that such changes in spin-down rate will not be discernible in the majority of objects which exhibit short-term ($\lesssim 1$ d) emission cessation. In light of this, we predict that many pulsars could exhibit similar magnetospheric and emission properties to PSR B0823+26, but which have not yet been observed.

Key words: methods: data analysis - pulsars: individual: PSR B0823+26 - pulsars: general.

1 INTRODUCTION

PSR B0823+26 was one of the first pulsars to be discovered (Craft et al. 1968) and, as such, has been studied for over 40 yr. Despite its typical spin parameters (i.e. rotational period $P \sim 0.53$ s, period-derivative $\dot{P} \sim 1.71 \times 10^{-15}$ and magnetic field strength $B \sim 0.96$ TG), this pulsar is by no means ordinary. Among its most salient features, are its inter-pulse and post-cursor emission components (Backer et al. 1973), which are typically observed at a few percent of its main-pulse peak intensity (Rankin 1986; see also Fig. 2). These features are quite rare among the pulsar population, particularly the inter-pulse emission which is only observed among a small subset ($\sim 3\%$; Maciesiak et al. 2011) of the normal pulsar population. PSR B0823+26 is also found to exhibit pulsed, soft X-ray emission (Becker et al. 2004), which makes it only one out of nine old pulsars ($1 \text{ Myr} < \tau < 20 \text{ Myr}$) that produce high-energy emission (e.g. Becker et al. 2004; Tepedelenhoğlu & Ögelman 2005; Li et al. 2008).

In addition to these rare emission features, the object exhibits abrupt cessation and re-activation of its radio emission (Hesse & Wiełebinski 1974; Ritchings 1976; Rathnasree & Rankin 1995), that is commonly referred to as ‘pulse nulling’ (Backer

1970). This phenomenon, which is also observed in numerous other pulsars, affects all components of emission (Backer 1970; Ritchings 1976) and can be thought of as an extreme manifestation of mode changing, that is a variation between active (radio-on, hereafter) and quiescent (radio-off or null, hereafter) emission modes. Through studying the emission behaviour of PSR B0823+26 over three observing runs ($\lesssim 2$ h of observations in total), Rathnasree & Rankin (1995) infer a *nulling fraction* (NF) – the fraction of pulses which are radio quiet – that is $6.4 \pm 0.8\%$.

While the documented nulls in PSR B0823+26 last a few pulse periods (Ritchings 1976), pulse nulling can be observed over a much wider range of timescales in pulsars; that is, from just one or two pulses to many days (e.g. Rankin 1986; Biggs 1992; Kramer et al. 2006; Wang et al. 2007). Accordingly, the NFs of pulsars can also range from less than 1% up to, in excess of, 95% (Deich et al. 1986; Wang et al. 2007). Due to this diversity in the observed nulling statistics, and incomplete sample of known objects which exhibit temporary radio emission failure – $\lesssim 200$ nulling (transient) pulsars are currently known, and even less have been studied in detail – not much is known about the ‘typical’ properties of nulling pulsars (e.g. P , \dot{P} or magnetic inclination an-

* Email: young.neiljames@gmail.com

gle α)¹, nor why exactly they undergo such extreme changes in their radio emission mechanism.

It has been suggested that ‘magnetospheric-state switching’ could be the underlying mechanism responsible for mode-changing and nulling in pulsars (e.g. Bartel et al. 1982; Contopoulos 2005; Timokhin 2010). This process refers to alterations to the global current distribution in a neutron star magnetosphere which, in turn, are thought to cause moding between different emission states. These global, magnetospheric reconfigurations are also proposed to explain the (quasi-)periodic timing signatures in pulsar residuals through correlated changes in spin-down rate ($\dot{\nu}$), such as those in the intermittent pulsar B1931+24 (Kramer et al. 2006; Hobbs et al. 2010; Lyne et al. 2010). However, not much is known about how such magnetospheric alterations are triggered, nor what their physical timescales or periodicities should be; there are a number of different models that attempt to explain this phenomenon, e.g. non-radial oscillations (Rosen et al. 2011), asteroid belts (Cordes & Shannon 2008), precessional torques (Jones 2012), surface temperature variations in the polar gap region (Zhang et al. 1997) and magnetic field instabilities (Geppert et al. 2003; Urpin & Gil 2004; Rheinhardt et al. 2004; Wang et al. 2007), but none are conclusive.

With the above in mind, we present the analysis of recent high-cadence observations of PSR B0823+26, which were stimulated by the discovery of longer than previously recorded nulls during regular timing observations with the Lovell Telescope at Jodrell Bank. These data represent the most comprehensive study of the intermittent behaviour of this pulsar for the first time. This subsequently enables the comparison between long-term intermittent pulsars and more ‘conventional’ nulling pulsars, as well as insight into the mechanism(s) which govern radio emission modulation in such objects. In Section 2, we describe the observations, followed by an overview of the emission variability of the source in Section 3. In Section 4, we review the timing behaviour of the neutron star, and the simulation tool used to model its rotational properties. Finally, we discuss the implications of the results in Section 5 and present our conclusions in Section 6.

2 OBSERVATIONS

The observations of PSR B0823+26, presented here, were obtained with the Lovell Telescope over a period of approximately 153 d (1 January 2009 to 3 June 2009). These data were obtained using the Analogue Filter Bank (AFB) and Digital Filter Bank (DFB)² back-ends using a 1400 MHz receiver, with an average cadence of approximately 4 observations per day (see Table 1 for details).

In addition to this typical daily monitoring, we carried out three observing runs with the AFB which spanned the entire time the source is above the horizon at Jodrell Bank (see Table 2 for details). These data were obtained to compare the long-term variation with possible short timescale modulation. As a result, there are significantly more observations with this back-end compared with the

Table 1. System characteristics of the observations of PSR B0823+26 described here. The bandwidth capability of the DFB was increased on 1 April 2009, i.e. MJD \sim 54922.1. Therefore, values quoted for the DFB back-end are with respect to times prior to (DFB_{pre}) and post (DFB_{post}) MJD \sim 54922.1 respectively.

| System Property | AFB | DFB _{pre} | DFB _{post} |
|--|-------|--------------------|---------------------|
| Time span of observations (d) | 153.3 | 77.3 | 60.9 |
| Total number of observations | 1274 | 284 | 281 |
| Typical observation duration (min) | 6 | 6 | 6 |
| Average observation cadence (d ⁻¹) | 8.3 | 3.7 | 4.6 |
| Typical sky frequency (MHz) | 1402 | 1382 | 1374 |
| Typical observing bandwidth (MHz) | 32 | 113 | 128 |
| Typical channel bandwidth (MHz) | 1 | 0.25 | 0.25 |

Table 2. The observation properties for the three continuous observing intervals during January 2009. Each continuous observing run has a length T_{obs} , for which there are N_{obs} separate observations.

| Start Epoch (MJD) | T_{obs} (d) | N_{obs} |
|-------------------|----------------------|------------------|
| 54837.7215 | 0.6390 | 152 |
| 54854.6844 | 0.6623 | 155 |
| 54857.7146 | 0.6067 | 145 |

DFB. Despite the deficit in the number of observations, the data obtained with the DFB is complementary to the emission modulation study due to the better sensitivity and wider bandwidth.

3 EMISSION VARIABILITY

3.1 Nulling activity and flux limits

The denser coverage provided by the AFB observations meant that they were used for characterising the overall emission modulation properties of PSR B0823+26. To determine whether the pulsar was radio-on or -off, we used the average profiles formed over the entire bandwidth for each approximately 6-min long observation. This was done by visual inspection and resulted in a time-series of one-bit data corresponding to the ‘radio activity’ of the pulsar i.e. 1’s for observations with detectable emission and 0’s for observations with non-detectable emission (i.e. radio-off states)³. To complement the visual inspection, we also made use of the timing model to confirm detections. A time-of-arrival (TOA) was calculated for each observation and was compared to the known timing model. Those in good agreement were confirmed as detections.

Figure 1 shows an example of an observation where the pulsar is observed to transition between the radio-on and radio-off phases. The transition timescales between the emission phases for this pulsar are similar to those seen in PSR B1931+24; that is, of the order of seconds or less. Such sharp discontinuities in pulse intensity are inconsistent with interstellar scintillation (see, e.g., Wang et al. 2005 and references therein). Therefore, these transitions between emission phases are considered to be intrinsic to the pulsar.

¹ While the NF of a pulsar is found to be weakly correlated with characteristic age (Rankin 1986; Wang et al. 2007), no significant correlation has been found with other basic pulsar properties or geometry (Rankin & Wright 2007).

² The DFB was commissioned approximately 20 d after the start of the AFB observations.

³ We note that only the nulling activity of the main-pulse component is considered here, as the 6-min observations do not provide enough sensitivity to characterise the inter-pulse or post-cursor emission properties.

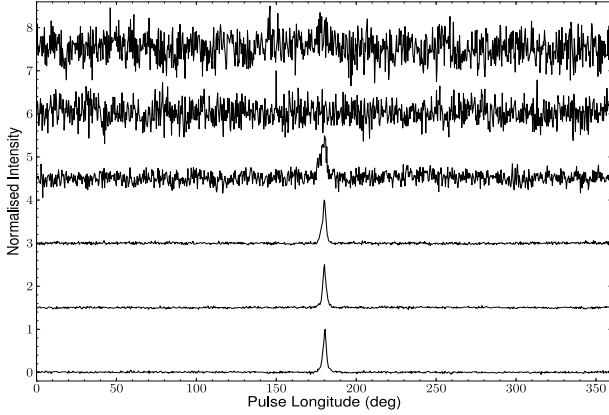


Figure 1. Consecutive pulse profile sub-integrations for PSR B0823+26 (from bottom to top), which were obtained during one observation on 10 May 2009. The pulse intensity of each sub-integration is normalised to one and is offset from the next profile for clarity. The pulsar is detectable in the first four sub-integrations (~ 60 s each), after which it abruptly ‘switches off’. This transition occurs sometime during the fourth sub-integration over a timescale of less than one minute.

Due to the greater sensitivity, we use the DFB data to provide limits on the average pulse flux density during the separate phases of emission. By considering an integrated profile, formed from an observation of length T , with an equivalent pulse width W_{eq} and signal-to-noise ratio SNR, the mean flux density can be estimated via the modified radiometer equation (e.g. Lorimer & Kramer 2005):

$$S = \frac{\beta \text{SNR} T_{\text{sys}}}{G \sqrt{n_p B T}} \sqrt{\frac{W_{\text{eq}}}{P - W_{\text{eq}}}}. \quad (1)$$

Here, $\beta \sim 1$ is the digitisation factor, $G \sim 1 \text{ JyK}^{-1}$ is the telescope gain, $T_{\text{sys}} \sim 35 \text{ K}$ is the system temperature, $n_p = 2$ is the number of polarisations, $B = 128 \text{ MHz}$ is the observing bandwidth, $P = 531 \text{ ms}$ is the pulsar period and $W_{\text{eq}} = 10 \text{ ms}$. We averaged a total of 202 radio-on and 6 radio-off observations, which correspond to total integration times of $T = 1174.2 \text{ min}$ and 33.6 min for the radio-on and -off phases respectively. The resultant time-averaged profiles are shown in Fig. 2. We place a limit on the mean flux density in a radio-off phase $S_{\text{off}} \leq 0.022 \pm 0.004 \text{ mJy}$ ($\text{SNR} \sim 3$), which is approximately 100 times fainter than that of the radio-on phase $S_{\text{on}} = 2.2 \pm 0.4 \text{ mJy}$ ($\text{SNR} \sim 1900$)⁴. Converting these parameters into pseudo-luminosities, using (Lorimer & Kramer 2005)

$$L_{1400} \equiv S_{1400} d^2, \quad (2)$$

we find $L_{1400, \text{off}} \lesssim 2.9 \mu\text{Jy kpc}^2$ and $L_{1400, \text{on}} \sim 0.29 \text{ mJy kpc}^2$ (where the pulsar distance $d \sim 0.36 \text{ kpc}$; Gwinn et al. 1986). We note that the pseudo-luminosity of PSR B0823+26 in the radio-off phase is at least six times fainter than the weakest known radio pulsar PSR J2144–3933 ($L_{1400} \sim 20 \mu\text{Jy kpc}^2$; Lorimer 1994). Although this implies that the radio-off phases are consistent with

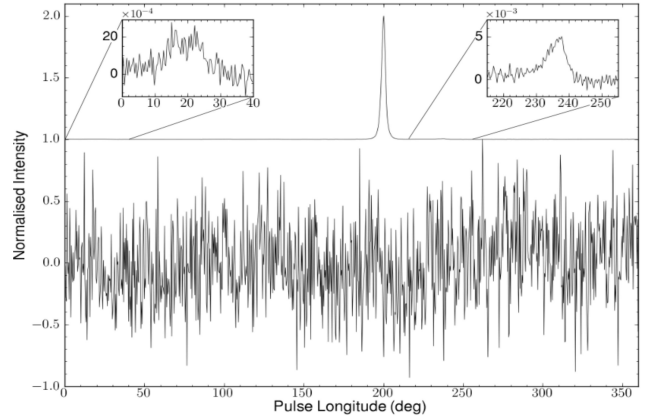


Figure 2. Average profiles of PSR B0823+26 for the radio-on (top) and radio-off (bottom) observations respectively, which are offset for clarity. The maximum pulse intensities are normalised to one. The inset plots show zoom-ins of the inter-pulse (left) and post-cursor (right) emission in the radio-on profile, using the same axes units as the main plot. Note that the y-axes of the inset plots represent the intensity offset from one.

emission cessation, we cannot rule out the possibility that they may exhibit extremely faint emission (c.f. Esamdin et al. 2005).

In Fig. 3, we show an ‘activity plot’, formed from the 153-d one-bit time-series data, which indicates when the pulsar was observed and whether it was radio-on or -off. The radio emission in PSR B0823+26 is clearly observed to undergo modulation over variable timescales, which are much shorter than those seen for PSR B1931+24 (i.e. days to weeks; Kramer et al. 2006).

The short-term emission modulation of PSR B0823+26 was probed using the data intervals of continuous observations, which are detailed in Table 2. These three data sets, shown in Fig. 4, display some evidence for ‘emission flickering’; that is, rapid changes between the radio-on and -off states of emission before a constant emission mode is assumed. We note, however, that further high-cadence observations are required to confirm this, and the typical characteristics of the ‘flicker’ pulses.

We also determined the emission phase durations for the object, which are defined as the difference between the start and end points (i.e. transition times) of emission phases. To reduce systematic error, the transition times for emission phases are assumed to be the mid-points between consecutive radio-on and -off observations, that is when the pulsar changes from radio-on to -off and vice versa. Fig. 5 shows the result of this analysis. These data clearly show that the distribution of radio-on phase durations exhibits a broader spread of values compared with that of the radio-off phase. Overall, however, there is a bias towards shorter emission phase durations, which is in stark contrast to PSR B1931+24. The average time that PSR B0823+26 exhibited detectable radio emission was $1.4 \pm 0.4 \text{ d}$. Whereas, the average radio-off timescale was $0.26 \pm 0.04 \text{ d}$. The activity duty cycle (ADC), the percentage of time in the radio-on phase, was calculated from the ratio of the total radio-on duration to the total observation time. The uncertainty in this value was determined from the ratio of the standard error in the radio-off time to the mean radio-off time. Subsequently, the pulsar is found to be radio-on for $80 \pm 10 \%$ of the time.

We were also interested in determining whether the pulsar exhibits any systematic trend in pulse intensity before (or after) a null (c.f. PSR B0809+74; Lyne & Ashworth 1983; van Leeuwen et al. 2002). Ideally, this analysis should be performed on single-pulse data. As these data were not available, however, we were limited to

⁴ We note that the value quoted here for the radio-on flux density is lower than that obtained by Lorimer et al. (1995) at 1400 MHz, i.e. $S_{1400} = 10 \pm 2 \text{ mJy}$. We attribute this discrepancy to our longer data set, which provides a more robust estimate due to the strong scintillation behaviour of the source (see, e.g., Wang et al. 2005).

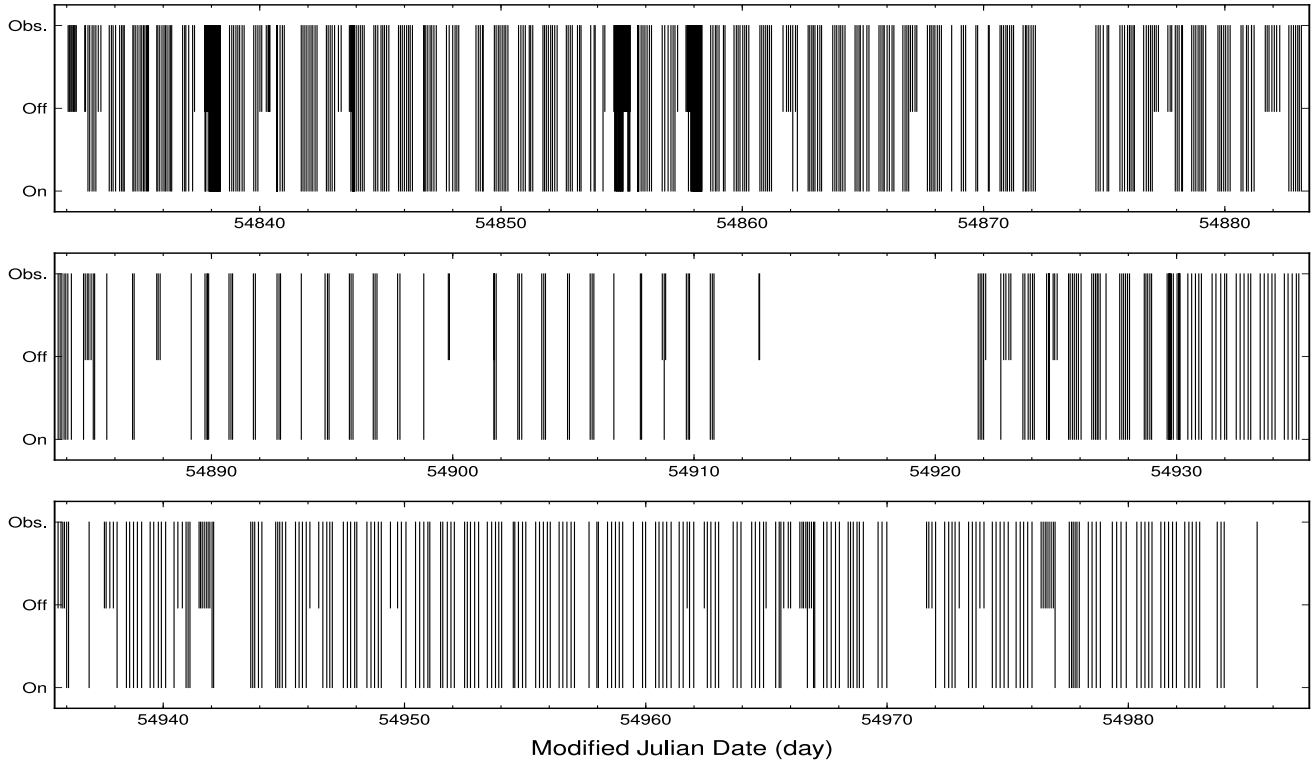


Figure 3. The sequence of observations of PSR B0823+26 carried out over the 153-d period, denoted by the black lines. The data are separated into three continuous $N \sim 54$ d panels. The times of observation and the times when PSR B0823+26 was radio-on (full-amplitude) and -off (half-amplitude) are shown by the extent of the black lines. The times of more intensive observing sessions are shown at MJD ~ 54838 , 54855 and 54858.

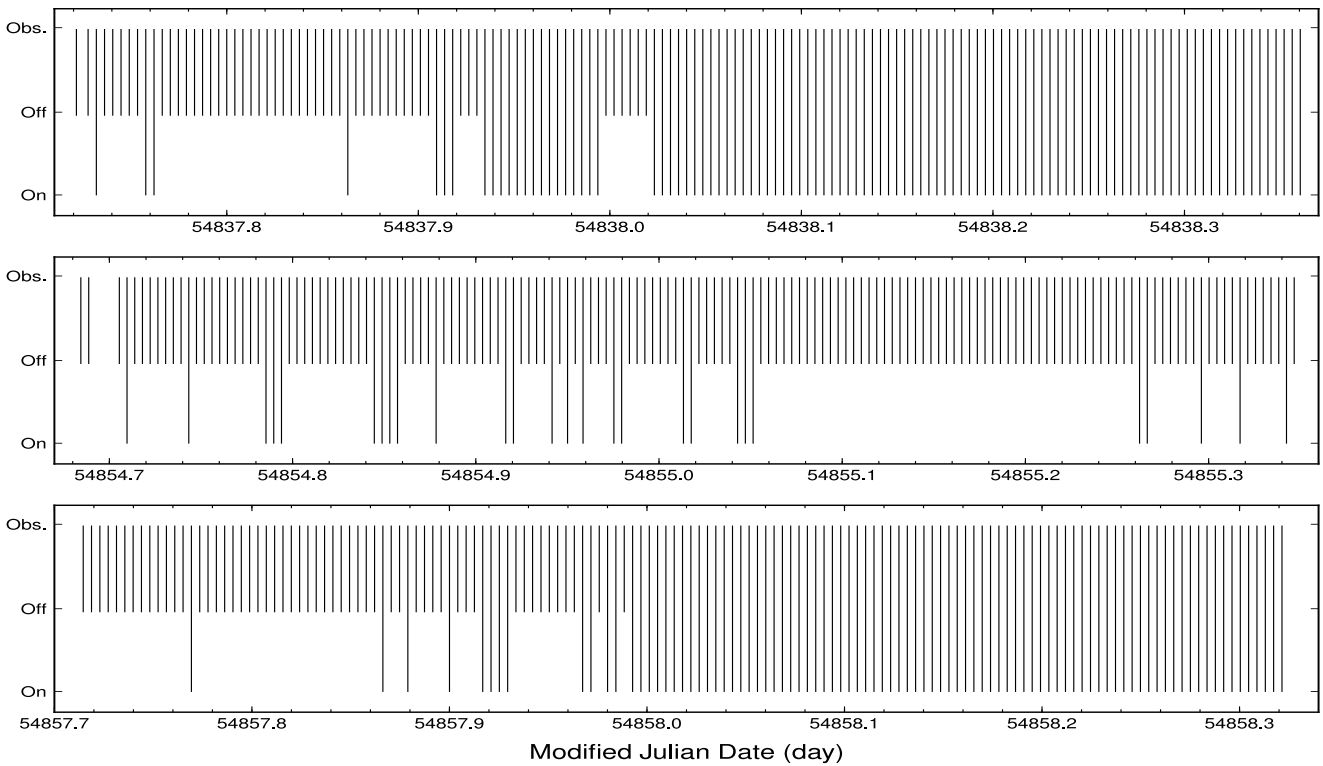


Figure 4. Three sequences of continuous observations of PSR B0823+26 during January 2009. The times when the pulsar was radio-on and -off are shown by the extent of the black lines.

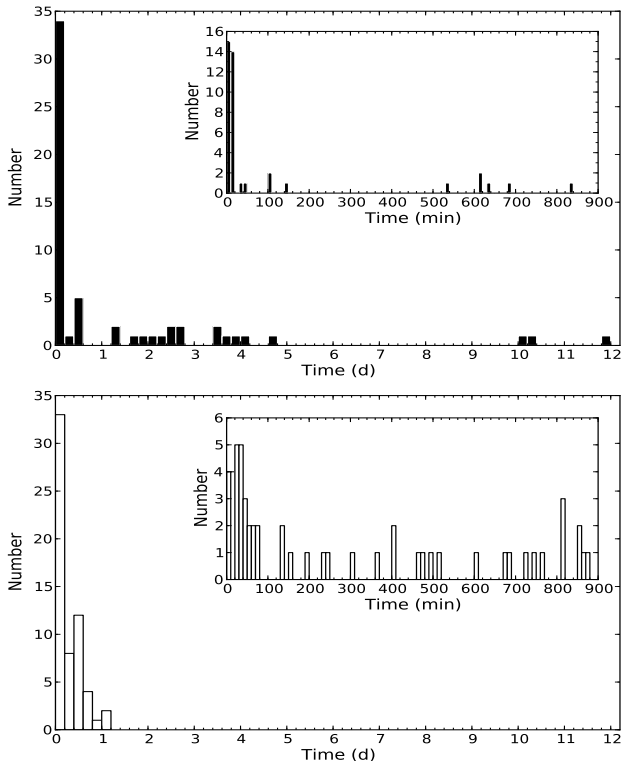


Figure 5. Histograms showing the durations of time when the pulsar is observed to be in a specific emission phase, on (*top*) and off (*bottom*), with inset plots of the radio emission activity for timescales up to 15 h.

using the 6-min integrated pulse profiles to discern any systematic brightness variations in the emission phases. We computed the peak flux density for each profile, using the first term in Eqn. 1, assuming a constant observing system (i.e. with stable T_{sys} , β and G parameters). We find no evidence to suggest any correlation between the pulse intensity and pulse integration number preceding (or following) a radio-off phase in these data. In addition, no correlation was found between emission phase length and pulse intensity.

3.2 Periodicity analysis

In order to elucidate the behaviour of PSR B0823+26, we have performed *weighted wavelet Z-statistic* (WWZ) analysis (Foster 1996) on the one-bit time-series data. The WWZ algorithm adopts a modified approach to traditional wavelet analysis (see, e.g., Addison 2002 for a review of wavelet transforms) in order to counter the undesired effects of uneven time sampling (e.g. spectral leakage; Scargle 1982). It employs a wavelet function which includes a periodic, sinusoidal test function, of the form $e^{i\omega(t-\tau)}$, by projecting the data onto a set of sine and cosine trial functions (i.e. the waveform). It also utilises a Gaussian window function (weighting function of the data) which is defined as (Foster 1996)

$$w(\omega, \tau) = e^{-c\omega^2(t-\tau)^2}, \quad (3)$$

and is centred at time τ , with a width defined by the frequency ω and tuning constant c .

As such, the WWZ uses the sinusoidal wavelet to fit the data and the sliding window function to weight the data points which, in turn, mitigates spectral leakage. We note here that data points towards the centre of the window in the fit are weighted the heaviest,

and those near the edges of the window the least. The spectral content of a signal is, subsequently, obtained at times corresponding to the centre of the wavelet windows (Bedding et al. 1998; Templeton 2004; Templeton et al. 2005).

For the purpose of our analysis, we chose $c = 0.001$ so that we could strike a balance between frequency and time resolution. The resultant WWZ transform of the one-bit time-series data, showing the spectral power at successive epochs (or *time lags*), is displayed in Fig. 6. It is clear that the WWZ transform exhibits very sporadic structure. This is thought to result from the effect of irregular data sampling on the projection (i.e. local matching) of the WWZ wavelet function. During the first ~ 40 d of the data-set, the observation sampling is at its greatest, with no gaps and $\sim 5 - 10$ observations per day (or more). The three continuous observing intervals are also included in this date range. Consequently, the data obtained over the first ~ 40 d accounts for $\sim 62\%$ of the total. We find that the data sampling in this observing period is sufficient for the matched wavelet function to return power at several fluctuation frequencies, which can be attributed to the locations of the continuous observing sessions. This is highlighted by the split in the WWZ data, centred around MJD ~ 54948 , which shows that the locations of dominant spectral features strongly correlate with the midpoints of the continuous observing sessions. The most prominent spectral feature can be seen at approximately $0.44 - 0.36 \text{ d}^{-1}$, corresponding to a period of about $2 - 3$ d. As the data sampling worsens with time, becoming more irregular (roughly a few observations per day) with occasional gaps (one is more than 10 d), there becomes a point at which the prominent fluctuation frequencies of the system are no longer resolved (i.e. around MJD ~ 54972).

In order to clarify the significance of these variations, we simulated several data-sets using the observed data sampling. We created model data-sets with single periodicities, ranging from 0.25 d to 10 d, and analysed them with the WWZ. We also performed WWZ analysis on data with randomised activity values. For the random data, the spectral power is distributed across the entire WWZ plane and no dominant periodicities are recovered. For the data with an intrinsic periodicity, however, we find that the fundamental frequency is resolved at virtually all epochs⁵. However, the fundamental spectral component is also accompanied by a broad distribution of power and is substantially less significant after the first 40 d⁶. For simulated periods of the order of a day, we note that the resulting distribution of power is similar to the broad distribution observed in the real data. This indicates that our results are modulated by data-windowing effects. We note that the higher period components in the observed data ($\sim 10 - 30$ d) are most probably not intrinsic to the pulsar. This is because the analysing wavelet has a full window-width (~ 10 cycles) that is of the order of the length of the data-set and, therefore, is not suitable to provide meaningful results about any long-term periodicity (Templeton 2004). These results suggest that there are a number of fluctuation frequencies present in the data, which are only resolved during epochs when there is the most frequent observation sampling. However, we are cautious to attribute these periodicities to the intrinsic variability of the source, due to the influence of the observation sampling on the results.

In order to elucidate the periodicities in the pulsar radio emis-

⁵ Around MJD $\approx 54913 - 54922$ there is a gap in the observations, which often results in a prominent decrease in the WWZ power.

⁶ The power relating to a time-frequency component in the WWZ represents its significance (Bedding et al. 1998).

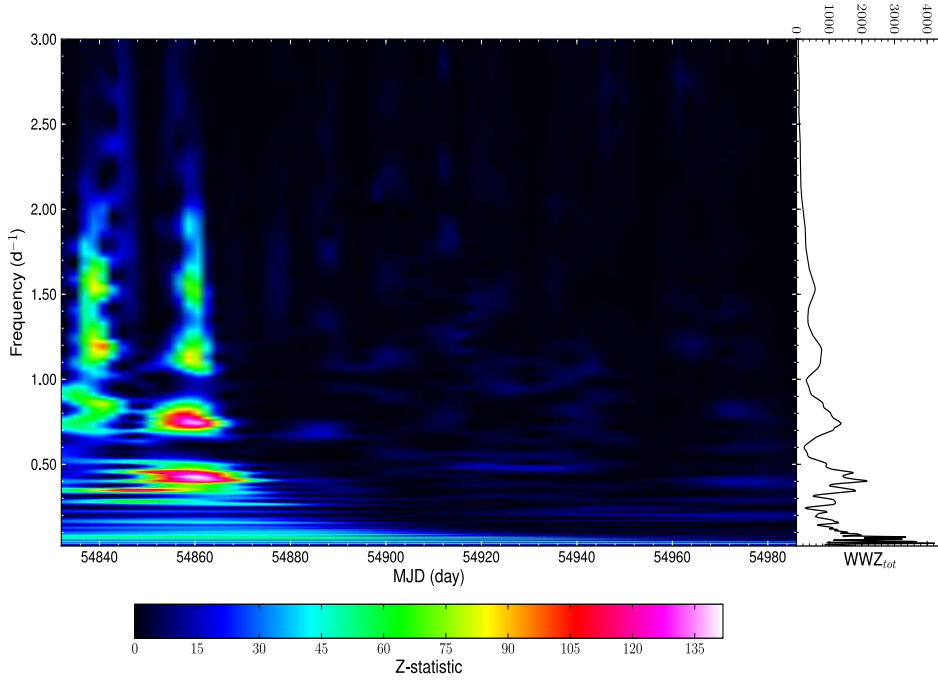


Figure 6. WWZ transform of the 153-d PSR B0823+26 radio emission activity data-set (*left*) and the corresponding integrated power spectrum (*right*). During the initial ~ 40 d of the data-set, the observation sampling is sufficient to resolve several prominent features. These spectral components are also accompanied by a broad distribution of power towards higher frequencies, which are likely analogous to Fourier harmonics. At later times ($\text{MJD} \gtrsim 54872$), the reduced data sampling does not allow insight into the dominant fluctuation frequencies.

sion, we now consider the error estimation of the WWZ data (Fig. 6). We note, however, that such error estimation is a non-trivial procedure. This is highlighted by Foster (1996), who state that analytic description of errors in a WWZ is very intricate, due to the nature of the weighted parametric projection. In addition, the assumptions made whilst devising the WWZ statistic practically invalidate the formal errors. For example, we assume the null hypothesis that the data is purely sinusoidal with constant frequency and amplitude, plus random noise, which we know is false. Therefore, any analytic errors which are calculated are consequently subject to these assumptions. As a result, we have applied a more heuristic approach to the estimation of WWZ errors. Here we employ two different methods, both of which are complementary.

3.2.1 Confusion limit estimation method

Following Templeton et al. (2005), we used the *confusion limit* method to estimate the peak fluctuation frequencies and their *maximum* $1\text{-}\sigma$ uncertainties. Here, the peak fluctuation frequency at a given epoch is one which is associated with the greatest WWZ power. The maximum $1\text{-}\sigma$ uncertainty associated with this frequency is approximated by measuring the confusion limit of the WWZ spectrum, that is the half-width at half-maximum of the Z-statistic, $Z(\omega, \tau)$. The result of this analysis is shown in Fig. 7. We find that the average error in the fluctuation frequency from this analysis is $\sim 11\%$.

The variation in the dominant periodicity, within the first 40 d, is above the error limit. However, as the data is clearly modulated by data-windowing effects (see above), we believe that these variations in the dominant periodicity are most likely governed by the observation sampling, rather than any modulation in the pulsar radio emission. Through comparing the observed data with the ran-

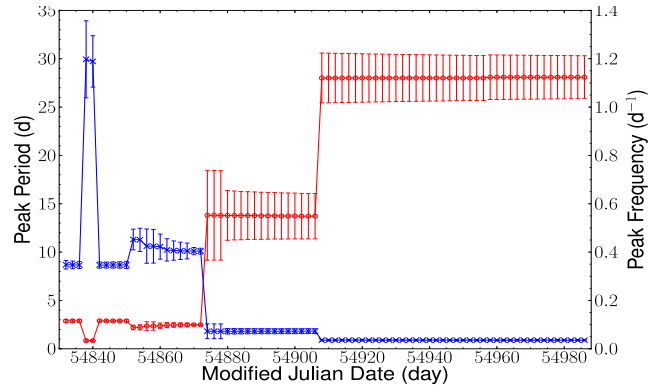


Figure 7. The peak fluctuation frequencies (*crosses*) and periods (*open circles*) from the weighted wavelet Z-transform data. Error bars are $1\text{-}\sigma$ values computed using the confusion limit estimation method (fractional errors for individual epochs). The average error in the peak fluctuation frequency (period) is $\sim 11\%$. For the first 40 d, the peak fluctuation period is typically $\sim 2 - 3$ d apart from at a couple of epochs (~ 0.8 d), which may represent a variation in the intrinsic periodicity. After $\text{MJD} \gtrsim 54872$, the data sampling becomes poorer, and more irregular, which favours the smaller (non-physical) peak fluctuation frequencies.

dom simulated data, we conclude that the source does exhibit some (quasi-)periodicity, but which cannot be accurately resolved here due to the aforementioned data-windowing effects.

3.2.2 Data-windowing method

Uncertainties in the WWZ transform were also estimated by computing the standard deviation of windowed data. Here, we separated

the WWZ data into segments of length $T = 14$ d, and calculated the standard deviation in the peak frequencies ($\sigma_{\nu(\tau)}$) and periods ($\sigma_{P(\tau)}$) for each segment accordingly. This provided a measure of the modulation in the peak frequency and period over time. We note, however, that we only included peak fluctuation periods which were below 10 d in this analysis, as these periods are the longest which are well represented by the WWZ (see above).

Table 3 shows the results of this analysis. The median peak fluctuation frequencies (periods) for the first three segments of the transform data are $\sim 0.42 - 0.35 \text{ d}^{-1}$ ($\sim 2 - 3$ d). We estimated the significance of periodicities within the WWZ data using a bootstrapping approach (e.g. Shao, J. & Tu, D. 1995; Politis, D.N. et al. 1999; Zoubir, A.M. & Iskander, D.R. 2004). Here, we resampled the transform data 100 times and, for each resample, determined the standard deviation. This allowed us to determine an accurate estimate for the average standard deviation, or background noise, of the transform data from the population of possible values. We assume a $5\sigma_{\text{WWZ}} \approx 80$ level as a confident signal detection. Consequently, we find that the median-peak WWZ values of the windowed data are significant for $\text{MJD} \lesssim 54872$. Whereas, those afterwards do not meet the cut-off criteria. This further indicates the importance of high-time resolution on the WWZ analysis; that is, periodicities in the data can only be accurately constrained when sufficient time resolution is available.

3.2.3 WWZ analysis summary

The above results indicate that PSR B0823+26 may exhibit a number of (quasi-)periodic features in its radio emission; the most prominent of these being around 2 – 3 d. However, evidence for their existence is only obtained during a small portion of the data-set (i.e. in the first 40 d), when the observation sampling is at its highest. From the simulated data-sets, it also appears that these ‘significant’ features may be influenced by spectral leakage (i.e. data-windowing effects on the WWZ). In light of this, we postulate that PSR B0823+26 does exhibit a fundamental (quasi-)periodicity in its radio emission, but stress that further higher-cadence observations are required to better characterise this behaviour.

4 TIMING BEHAVIOUR

In PSR B1931+24, we see systematic variations in its timing residuals, which manifest as quasi-periodic cubic structure due to spin-down rate variation (Kramer et al. 2006). To determine whether PSR B0823+26 exhibits similar behaviour, we analysed the timing measurements obtained from the 153-d AFB data-set. We obtained the topocentric TOAs using PSRPROF⁷ and analysed them using the TEMPO2 package⁸. The resulting residuals (observed – predicted TOAs) from a best-fit timing model (Table 4) are shown in Fig. 8.

We find that there is no significant evidence for any periodicity in the 153-d AFB timing residuals. However, this is not that surprising considering the timescales of emission variation (\sim hours) will result in an observational bias against such detection; the ability to resolve a discrepancy between observed and predicted TOAs will be strongly dependent on the length of time a

Table 4. The properties of PSR B0823+26 obtained from timing measurements of the 153-d AFB data-set. Note that the right ascension, declination and dispersion measure of the source are held fixed in the fit to these data. The standard 1- σ errors are provided in the parentheses after the values, in units of the least significant digit.

| Parameter | Value |
|---|---|
| Right Ascension (J2000) | $08^{\text{h}} 26^{\text{m}} 51^{\text{s}}.489$ |
| Declination (J2000) | $+26^{\circ} 37' 23''.706$ |
| Epoch of frequency (modified Julian day) | 54909.0 |
| Rotational frequency ν (Hz) | $1.884439516337(1)$ |
| Rotational frequency derivative $\dot{\nu}$ (s^{-2}) | $-5.997(1) \times 10^{-15}$ |
| Dispersion Measure DM ($\text{cm}^{-3} \text{ pc}$) | 19.464 |

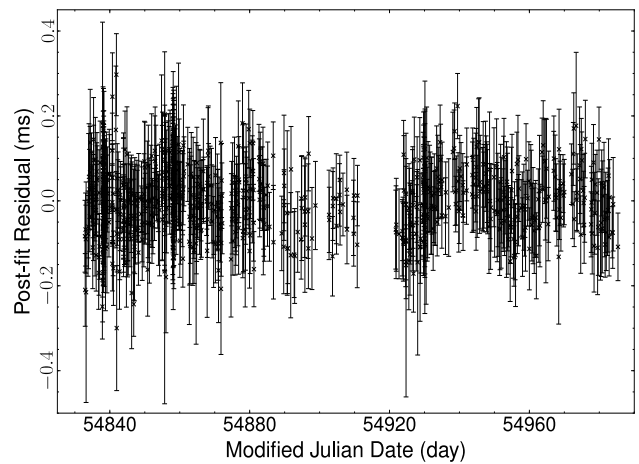


Figure 8. Post-fit timing residuals for PSR B0823+26 from the 153-day AFB data-set, after fitting for ν and $\dot{\nu}$. There is no apparent cubic structure in the timing residuals.

pulsar assumes a given spin-down rate. Nevertheless, it is possible that the object alternates between spin-down rates, consistent with the magnetospheric-state changing scenario (Lyne et al. 2010), but we are not sensitive to the variations in the timing residuals. This idea will be explored in greater detail in the following sections.

4.1 Overview of the timing model

To determine whether the timing measurements of PSR B0823+26 could be consistent with a variable spin-down model, we developed a simulation tool to reproduce the timing behaviour of intermittent pulsars. This tool is based on a Monte-Carlo method, whereby we define a parameter space of trial radio-on and -off spin-down rates ($\dot{\nu}_{\text{on}}$ and $\dot{\nu}_{\text{off}}$) to produce simulated timing residuals that are compared with the observed. The tool also uses an initial rotational frequency, ν_0 , and average fitted rotational frequency derivative, $\dot{\nu}_{\text{av}}$, to simulate the timing behaviour of the object. These additional parameters are determined from fitting the pulsar’s rotational and orbital parameters from the observed data using TEMPO2 (see Table 4).

The emission activity of the source is represented by two analytic, exponential functions that separately model the observed distributions of emission phase durations (i.e. radio-on and -off). The pulsar is modelled to sequentially switch between the radio-on and -off phases. Therefore, the simulated emission phase durations are obtained from the analytic functions by alternately and randomly

⁷ <http://www.jb.man.ac.uk/pulsar/observing/progs/psrprof.html>

⁸ A detailed overview of this timing package is provided by Hobbs et al. (2006). Further details and documentation can also be found at <http://www.atnf.csiro.au/research/pulsar/tempo2/>.

Table 3. Summary of the results from the data-windowing error analysis. The time span of the WWZ data analysed is denoted by ‘MJD range’. The median-peak WWZ values, of these segments, and their 1- σ uncertainties are denoted by WWZ_{\max} and $\Delta(WWZ_{\max})$ respectively. The peak fluctuation frequencies, periods and their corresponding 1- σ uncertainties are given by ν_{fluc} , $\Delta(\nu_{\text{fluc}})$, P_{fluc} and $\Delta(P_{\text{fluc}})$ respectively.

| MJD range | WWZ_{\max} | $\Delta(WWZ_{\max})$ | $\nu_{\text{fluc}}(\text{d}^{-1})$ | $\Delta(\nu_{\text{fluc}})(\text{d}^{-1})$ | $P_{\text{fluc}}(\text{d})$ | $\Delta(P_{\text{fluc}})(\text{d})$ |
|-------------|--------------|----------------------|------------------------------------|--|-----------------------------|-------------------------------------|
| 54832–54846 | 94 | 25 | 0.35 | 0.39 | 2.9 | 1.0 |
| 54846–54860 | 125 | 9 | 0.42 | 0.05 | 2.4 | 0.3 |
| 54860–54874 | 113 | 32 | 0.40 | 0.12 | 2.5 | 4.0 |
| 54874–54888 | 63.9 | 0.2 | 0.0728 | 0.0001 | 13.79 | 0.02 |
| 54888–54902 | 62 | 1 | 0.0728 | 0.0001 | 13.75 | 0.02 |
| 54902–54916 | 57 | 1 | 0.04 | 0.02 | 28.0 | 7.4 |
| 54916–54930 | 57.4 | 0.3 | 0.0357 | 0.0000 | 28.0 | 0.0 |
| 54930–54944 | 58.0 | 0.1 | 0.0357 | 0.0000 | 28.0 | 0.0 |
| 54944–54958 | 58.1 | 0.1 | 0.03570 | 0.00004 | 28.01 | 0.03 |
| 54958–54972 | 57.5 | 0.3 | 0.0356 | 0.0000 | 28.09 | 0.00 |
| 54972–54986 | 56.3 | 0.5 | 0.0356 | 0.0000 | 28.09 | 0.00 |

sampling from the possible ranges of values. This process is continued until the emission activity of the total observed data duration (~ 153 d) is fully covered for each simulation trial, thus producing pseudo-random generated number distributions for both the radio-on and -off emission phase durations. This method, in turn, provides us with a better general description of the pulsar emission activity, due to the finite number of data points we can sample from the parent distributions. With the above in mind, the timing residuals of each simulation trial represent one possible observed outcome, for a given pair of spin-down rates, considering a pulsar which exhibits variable emission activity with given distributions of switch durations.

As the spin-down rate of the model pulsar alternates between consecutive emission phases, the rotational frequency is updated at each integer step in pulse number:

$$\text{TOA} = \frac{n}{\nu} + t_{\text{ref}}. \quad (4)$$

The reference time t_{ref} corresponds to the total time elapsed at the last step and n is the number of pulses in each emission mode. The rotational frequency ν is updated using

$$\nu = \nu_{\text{ref}} + (\dot{\nu}_{\text{phase}} \times \Delta t), \quad (5)$$

where ν_{ref} is the reference frequency at the last step, $\dot{\nu}_{\text{phase}}$ is the spin-derivative in the corresponding emission phase and Δt is the duration of the emission mode.

The simulated TOAs, obtained from these data, are those that would be measured at the Solar System Barycentre (Barycentre reference frame) and are inclusive of additive white Gaussian noise, to simulate instrumental noise. For each simulated TOA, the noise signature is calculated from a randomly selected error bar from the observed data; a random number is generated from a Gaussian distribution with a full-width at half-maximum that is twice the size of the error bar. To track pulsar rotation in time, TOAs for radio-on and -off phases are calculated. The radio-off phase TOAs are the theoretical TOAs which an observer would measure if the pulsar was detectable.

We note here that, as ν is evolved over time, the initial value for this quantity is equal to the rotational frequency at the start point of each simulation trial ν_0 , which is obtained from the average ν of the observed data. Therefore, for each combination of $\dot{\nu}_{\text{on}}$ and $\dot{\nu}_{\text{off}}$, the simulated value for ν_0 will be different compared to the observed due to the relative contributions of $\dot{\nu}_{\text{on, off}}$. This, in turn, results in a systematic offset in the resulting timing residuals. To

correct for this effect, we fit an average ν to each set of simulated timing residuals using TEMPO2. It is important to note that we only consider the radio-on phase TOAs in these fits, so as to accurately simulate the observations. Following this procedure, we then use TEMPO2 to provide post- ν -fit root-mean-square (hereafter, simply referred to as RMS) values for each $\dot{\nu}_{\text{on, off}}$ trial combination. The optimal combination of $\dot{\nu}_{\text{on}}$ and $\dot{\nu}_{\text{off}}$ is then taken as that which obtains an average RMS from these trial values which is closest to the observed.

4.2 Simulation analysis

To calibrate the simulation tool, and test its functionality, it was applied to the prototype intermittent pulsar PSR B1931+24. Kramer et al. (2006) show that there is clear quasi-periodic, cubic structure in the timing residuals of this pulsar and fit the data to obtain $\dot{\nu}_{\text{on}} = -16.3 \pm 0.4 \times 10^{-15} \text{ s}^{-2}$ and $\dot{\nu}_{\text{off}} = -10.8 \pm 0.2 \times 10^{-15} \text{ s}^{-2}$. As a consistency check, we analysed the same data-set using a number of trial spin-down rates within the stated uncertainties. TOAs obtained between 4 May 2003 and 9 October 2003 with the Lovell telescope were analysed using TEMPO2 to determine ν_0 and $\dot{\nu}_{\text{av}}$, and to create an accurate ephemeris, to perform the analysis. We find that the simulation tool reproduces the timing behaviour of PSR B1931+24 well, as shown in Fig. 9, for $\dot{\nu}_{\text{on}} = -16.1 \times 10^{-15} \text{ s}^{-2}$ and $\dot{\nu}_{\text{off}} = -10.8 \times 10^{-15} \text{ s}^{-2}$. We note here that there are a couple of small offsets between the observed and simulated residuals (at MJD ~ 52820 and ~ 52918), but emphasise that these do not reflect on the validity of the simulation tool. We stress that the example shown (Fig. 9) does not represent a perfectly optimised result. It is also important to note that the emission phase durations of PSR B1931+24 are only known to an accuracy of approximately ± 1 d. This, in turn, will naturally result in a discrepancy between the observed and simulated data, if the actual timescales of emission are different to those determined by the observation sampling.

Following the above approach, we obtained ν_0 and $\dot{\nu}_{\text{av}}$ for PSR B0823+26. We determined the constraints on the combinations of $\dot{\nu}_{\text{on}}$ and $\dot{\nu}_{\text{off}}$ from the pulsar’s ADC and average fitted $\dot{\nu}$, which by definition is

$$\dot{\nu}_{\text{av}} = (t_{\text{on}} \times \dot{\nu}_{\text{on}}) + (t_{\text{off}} \times \dot{\nu}_{\text{off}}), \quad (6)$$

where t_{on} and t_{off} are the fractional times that the pulsar is in the radio-on and -off emission phases respectively. Accord-

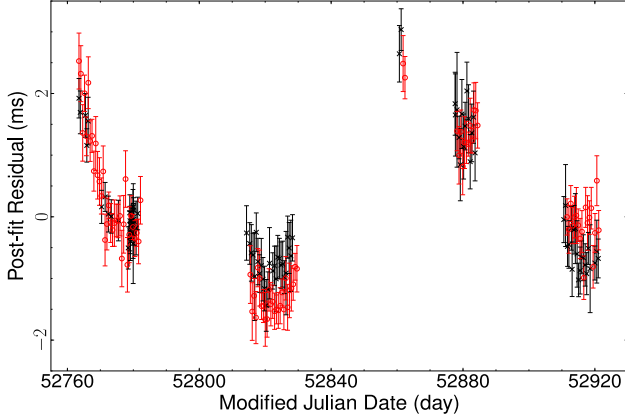


Figure 9. Observed (*crosses*) and simulated (*open circles*) timing residuals of PSR B1931+24, using the same data as that in Kramer et al. (2006) but with slightly different spin parameters. The results of the simulation are consistent with the timing behaviour of the source.

ingly, the parameter space of spin-derivatives to test was defined as $-6.06 \leq \dot{\nu}_{\text{on}} (10^{-15} \text{ s}^{-2}) \leq -5.99$ and $-6.0 \leq \dot{\nu}_{\text{off}} (10^{-15} \text{ s}^{-2}) \leq -5.6$ (assuming a small variation in the spin-down rate between emission phases). The spin-derivatives are inherently constrained by $\dot{\nu}_{\text{av}} \sim -5.997 \times 10^{-15} \text{ s}^{-2}$, so that neither $\dot{\nu}_{\text{on}}$ or $\dot{\nu}_{\text{off}}$ can cross this boundary. For each combination of input parameters, the RMS was calculated for 2000 iterations of the simulation tool using a resolution of $2 \times 10^{-18} \text{ s}^{-2}$ in $\dot{\nu}_{\text{on, off}}$. These data were then averaged and compared with the RMS and measured uncertainty from the observed data. The uncertainty was calculated using TEMPO2 to fit the observed data across individual segments. Here, the average and standard deviation of the sample population of observed RMS values were computed, and then used to obtain the fractional error and measured uncertainty in the RMS. Assuming a $3\text{-}\sigma$ error in the observed RMS, we obtain a constraint of $\text{RMS} = 80 \pm 10 \mu\text{s}$ on the simulated results.

The result of this analysis can be seen in Fig. 10. The parameter space of $\dot{\nu}_{\text{on}} - \dot{\nu}_{\text{off}}$ where the RMS converges on the observed value is seen to be distributed, within the observational errors, towards the central diagonal portion of the plot. This can be attributed to Eqn. 6, which shows that $\dot{\nu}_{\text{av}}$ of the simulated data, and hence the RMS by logical progression, will converge with the observed for $\dot{\nu}_{\text{on}} \propto 1/\dot{\nu}_{\text{off}}$. Consequently, we find that the maximum increase from $\dot{\nu}_{\text{off}}$ to $\dot{\nu}_{\text{on}}$ ($\Delta\dot{\nu}_{\text{max}}$) which satisfies the model criteria is approximately 6%.

We also note that as the emission phase durations are sampled randomly from the model distributions, there exists a variance in the computed average RMS for each combination of input parameters. As such, we find that the results of the simulation tool are less variable for $\dot{\nu}$ values which are closer to the observed average; the variance in the results from the simulated residuals has to be smaller for the simulation to be consistent with the observations. Despite the fact that the simulation tool can be applied to any intermittent pulsar, it is ideally suited to modelling those with small $\Delta\dot{\nu}$ as least-squares fitting methods, such as the method implemented by Kramer et al. (2006), will be more efficient for larger $\Delta\dot{\nu}$. That is, the simulation tool can provide an upper limit to $\Delta\dot{\nu}$, which is independent of curve-fitting analyses which are unfeasible when analysing timing signatures with negligible cubic structure.

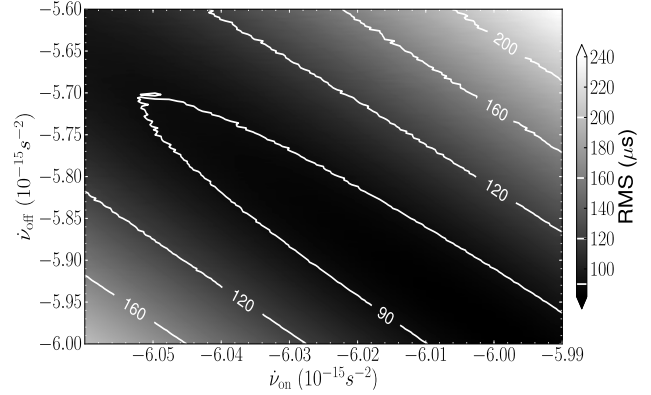


Figure 10. Residual contour map obtained from simulations of the timing behaviour of PSR B0823+26, for given combinations of rotational frequency derivatives. The plot shows the distribution of RMS values for the specified range of $\dot{\nu}_{\text{on, off}}$, with the contours denoting RMS levels for the given parameters. The diagonal region in the middle of the plot shows the area of acceptable $\dot{\nu}$ combinations. The observed timing RMS is $80 \pm 10 \mu\text{s}$.

4.3 Switching timescale dependency

Further to the analysis of the simulated data, the effects of altering the emission phase durations and ADC were investigated. We were interested in determining whether our results were subject to systematic effects and how they were affected by modelling the emission behaviour differently.

Firstly, we investigated the effect of over or under-estimating the observed emission phase durations. We added systematic errors to the observed durations, t_{obs} , with a magnitude from 0% to 100% in steps of 5%, with the polarity of the error (for each emission mode) being determined by a random number generator. As the percentage error was increased, the average RMS over 2000 iterations of the simulation tool was found to increase also. That is, as the variance in the emission phase durations increases, so do the fluctuations in the timing residuals due to the model pulsar assuming a spin-down rate for longer or shorter than is observed. We find that the tolerance of the RMS to these systematic errors increases towards smaller variations in the spin-down rate. This is particularly true for the combinations of spin-parameters which were comparable with the average spin-down rate; the results of the simulation remained consistent with the observed even for an error of $\pm 100\%$ in the emission phase durations.

To confirm the validity of the maximum allowed change in spin-down rate, $\Delta\dot{\nu}_{\text{max}} \sim 6\%$, we also performed a simulation trial using the observed switching times without any systematic errors. Here, we used the corresponding values for $\dot{\nu}_{\text{on, off}}$ which resulted in the maximum spin-down rate variation. From this analysis, we obtain an RMS which is greater than that observed. However, this result is only derived from one trial and, as such, is not expected to be as consistent as averaging over many simulated results. In addition, the value quoted for $\Delta\dot{\nu}_{\text{max}}$ inherently serves as an upper limit. Therefore, it is possible that the pulsar may undergo more modest variations in its spin-down rate; simulations incorporating these spin-parameters produce results that are more consistent with observations. We note, however, that systematic errors in the observed emission durations will have a significant effect on the $\Delta\dot{\nu}_{\text{max}}$ limit obtained. As a result, we argue that timing studies of intermittent pulsars will be more conclusive for better sampled data-sets.

We also tested our assumption that the emission activity of PSR B0823+26 can be modelled by randomly sampling two distributions of emission phase durations. Here, we compare the results of separate trials which used the analytic and observed (both ordered and randomised) sequences of emission phase durations. We find that the average RMS values from these trials are all consistent. Therefore, we conclude that the assumptions of our simulation tool are valid.

In addition, we examined the dependency of the results on the ADC assumed. In this analysis, the sequences of radio-on and -off emission phase durations were combined together and randomised, so that no distinction was made between the different distributions. This, in turn, resulted in an ADC which no longer coincided with the observed value, that is $\sim 50\%$. A number of $\dot{\nu}$ combinations were used in this analysis, from $\Delta\dot{\nu}_{\min}$ to $\Delta\dot{\nu}_{\max}$. However, no RMS values within the observed $80 \pm 10 \mu\text{s}$ could be obtained (except for $\dot{\nu}_{\text{on}} \sim \dot{\nu}_{\text{off}}$). This indicates that the form of the distribution which is used to model the emission phase durations is fundamental to the simulation procedure.

To investigate this further, and to determine how unique the $\Delta\dot{\nu}_{\max}$ solution is, the analytic distributions of emission phase durations were also directly altered. Here, simulations were carried out where the parameters of the distributions were modified to obtain two test cases, for $\sim 5\%$ decrease and increase in the ADC. These simulations returned $\dot{\nu}_{\text{on,off}}$ matches that corresponded best with the ADC. That is, for an approximately 5% decrease in the ADC, the maximum change in the spin-down rate reduces, and vice versa. For a lower percentage radio-on time, $\Delta\dot{\nu}$ is required to be smaller to obtain $\dot{\nu}_{\text{av}}$, and the opposite for a higher percentage. As a result, we obtain limits on the maximum change in spin-down rate $4.5\% \lesssim \Delta\dot{\nu}_{\max} \lesssim 7.6\%$, if we assume a maximum error of $\sim 5\%$ in the modelling of the random number distributions. Consequently, we see that alteration to the ADC has a significant effect on the results; if the initial parameters used are wrong, the simulation tool will not converge on an optimum combination of spin-down rates. Despite the incorporation of a 5% uncertainty in the ADC, it is apparent that the upper limits on the spin-down rate variation are still small compared with that of PSR B1931+24 ($\sim 50\%$; Kramer et al. 2006).

5 DISCUSSION

5.1 Nulling timescales in PSR B0823+26

While our data represent the most comprehensive study of the long-term nulling behaviour of PSR B0823+26, we suspect that the majority of the inferred nulling timescales are influenced by data-windowing effects. That is, we predict that the emission phase durations are often overestimated due to insufficient time coverage. This is strongly supported by the activity plots (Fig. 3 – 4) which, when compared, clearly show that the pulsar exhibits a much shorter modulation timescale (\sim minutes to hours) than can be resolved in the typical observing cadence (\sim days). This effect also influences the result of the WWZ analysis (Fig. 6), due to the lack of any significant spectral features at times of poor observation cadence. Therefore, we cannot explicitly state the *typical* modulation timescale(s) intrinsic to PSR B0823+26; it is likely that the sparser sampling of the typical observations may have resulted in missing numerous radio-on and -off states.

Although the majority of our data is subject to the data-windowing effects mentioned above, the data from the continuous

observing runs is not. Therefore, we can use these data to place confident limits on the short-term variability of PSR B0823+26. In light of this, we conclude that the source undergoes nulls over timescales of minutes to hours (up to at least 5 h), but do not rule out the possibility of longer (~ 1 d) null phases, which require further investigation. Remarkably, in these observing runs, we also find evidence for highly irregular short-term ($\lesssim 1$ h) modulation. That is, the object appears to exhibit periods of spontaneous bursts of emission and nulls, or emission flickering, before a constant emission phase is assumed. If this is typical for neutron stars, it may be inferred that pulsars which exhibit intermittency, e.g. normal nulling pulsars and rotating radio transients (RRATs; McLaughlin et al. 2006), may undergo a radio emission ‘ignition phase’ before attaining the necessary criteria for stable emission⁹. However, this behaviour could just be intrinsic to PSR B0823+26 and, therefore, requires the study of other sources to associate it to the pulsar population as a whole. Evidently, this would be complemented by further investigation into the typical nulling behaviour of PSR B0823+26, which may provide insight into this phenomenon and the mechanism(s) responsible for emission modulation in pulsars.

Taking in mind that nulling pulsars exhibit null durations of 1 – 10 pulse periods up to approximately a year (PSR J1841–0500; Camilo et al. 2012), PSR B0823+26 may be considered to be a bridge between the different ‘types’ of nulling pulsars. That is, the object may be located inbetween conventional nulling pulsars and longer-term intermittent pulsars on a ‘nulling continuum’ scale (Keane 2010). A question to now ask then, is if these sources all show different cessation timescales will all of them exhibit $\Delta\dot{\nu}$ and, if so, how will it manifest? This will be investigated in greater detail below.

5.2 Evidence and implications of $\Delta\dot{\nu}$ in PSR B0823+26

For the first time, we have presented a simulation tool which can model the timing behaviour of an intermittent pulsar and obtain an upper limit on its spin-down rate variation. Through simulating the rotational behaviour of PSR B0823+26, we find $\Delta\dot{\nu}_{\max} \sim 6\%$ between emission phases, which corresponds to $\dot{\nu}_{\text{on}} = -6.05 \times 10^{-15} \text{ s}^{-2}$ and $\dot{\nu}_{\text{off}} = -5.702 \times 10^{-15} \text{ s}^{-2}$. However, we cannot discount a scenario where there is no variation in spin-down rate between the different radio emission phases. Keeping this in mind, we can still try to estimate the implied current flow in the pulsar magnetosphere for both the radio-on and -off states using the above values. We follow Kramer et al. (2006) and consider the simplest possible emission model. That is, we assume that in the radio-off state the pulsar spins down by a mechanism that does not involve substantial particle ejection (e.g., via magnetic dipole radiation if the pulsar is in vacuum). Whereas, in the radio-on state, we assume that spin-down rate is enhanced by a torque from the current of an additional plasma outflow. Modifications of this simple assumption are possible (e.g. considering the spin-down contribution of a plasma-filled close-field line region, see Li et al. 2012a), but for our purposes the simplest model is sufficient. Hence, with the assumption that the increase of the spin-down rate is purely due to the torque of the charged plasma additionally existing in the radio-on state, over the radio-off state vacuum spin-down, one derives an estimate for the charge density

⁹ In this context, RRATs may never attain the criteria for stable emission.

of this wind component:

$$\rho_{\text{plasma}} \approx \frac{3I \Delta \dot{\nu} c^2}{1.26 \times 10^{21} R^6 \sqrt{\nu \dot{\nu}_{\text{off}}}} \sim 0.0024 \text{ C m}^{-3}, \quad (7)$$

where c is the speed of light in a vacuum, R is the radius of the pulsar (taken to be 10^6 cm) and I is the moment of inertia (assumed to be 10^{38} kg m²). We note that this equation also assumes that the object is an orthogonal rotator, i.e. the source has a magnetic inclination angle of 90° . While this assumption is almost certainly not met for most sources, this seems to be indeed a good approximation for PSR B0823+26 ($\alpha \sim 86^\circ$; Everett & Weisberg 2001)¹⁰. Comparing the above estimate with the Goldreich-Julian density, i.e. the screening density in a simple dipolar spin-down model (e.g. Lorimer & Kramer 2005)

$$\rho_{\text{GJ}} = \frac{B_s \nu}{c} \sim 0.0203 \text{ C m}^{-3}, \quad (8)$$

where B_s is the surface magnetic field strength of the pulsar, we at least obtain a good indication that only a small amount ($\sim 12\%$) of the total available charge in the wind component is contributing to the overall spin-down. This indicates that the open field line region of the pulsar magnetosphere may never become entirely depleted of charge during a radio-off phase (c.f. Li et al. 2012a) or, alternatively, that the spin-down of the pulsar is dominated by the non-wind contribution (i.e. magnetic dipole radiation).

For PSR B1931+24 it is suggested that the radio emission cessation results from re-configuration of the global magnetospheric charge distribution, and that the spin-down rate variation is a signature of this phenomenon (Kramer et al. 2006; Timokhin 2010; Lyne et al. 2010; Li et al. 2012a,b). Certainly, in several other pulsars, we see evidence to support this theory (Lyne et al. 2010). However, it is not entirely clear what manner of emission modulation will be accompanied by a variable spin-down rate; in the study performed by Lyne et al. (2010), pulsars with similar changes in spin-down rate were observed to undergo different magnitudes of variation in their pulse shape. It is interesting, therefore, to find that PSR B0823+26 exhibits the same breakdown in radio emission production (or detectability) as PSR B1931+24, without the need for a large change in the magnetospheric currents. This implies that the mechanism which produces radio emission is highly sensitive to even the smallest changes in the magnetosphere and that mode-changing and nulling are closely related. From this, we infer that there could be a significant number of pulsars that exhibit regulated changes in their spin-down rate and emission, which contribute to ‘timing noise’, and that we are not yet aware of them due to small fractional changes in $\dot{\nu}$ or short timescale variations.

5.3 Detection limits on $\Delta \dot{\nu}$

While a large number of pulsars are thought to exhibit spin-down rate variation (Hobbs et al. 2010; Lyne et al. 2010), only 20 are known to exhibit any discernible change in $\dot{\nu}$ (e.g. Kramer et al. 2006; Lyne et al. 2010; Camilo et al. 2012). With this in mind, we sought to determine our sensitivity to $\Delta \dot{\nu}$ in neutron stars and, hence, whether we can expect to detect this effect in all mode-changing and nulling pulsars.

We begin by considering a simple model of a dual- $\dot{\nu}$ nulling

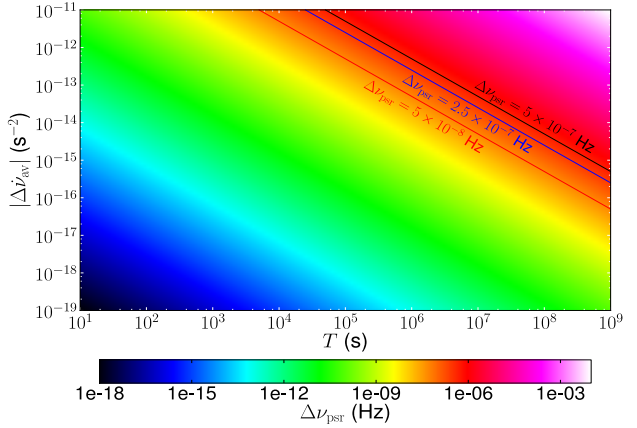


Figure 11. The expected change in rotational frequency, $\Delta \nu_{\text{psr}}$, due to an average spin-down rate deviation, $|\Delta \dot{\nu}_{\text{av}}|$, that is assumed for a time T . Overlaid are lines denoting the possible detection requirements of a variable spin-down rate in PSR B0823+26, that is (from left to right) $\Delta \nu_{\text{mod}}$, $5 \Delta \nu_{\text{mod}}$ and $10 \Delta \nu_{\text{mod}}$.

pulsar, which alternately exhibits $\dot{\nu}_{\text{on}}$ and $\dot{\nu}_{\text{off}}$ in its corresponding emission phases, for a given length of time Δt_i . If the data is fitted with a standard timing model with a single value of $\dot{\nu}$ ($\dot{\nu}_{\text{av}} = \dot{\nu}_{\text{pred}}$; see, e.g., Manchester & Taylor 1977), we expect the total difference between the observed and predicted spin-down rates, in each emission phase, to be $\Delta \dot{\nu}_i = \dot{\nu}_{\text{obs}} - \dot{\nu}_{\text{pred}}$. Extending this model to N emission phases, we would expect the total discrepancy between the observed and predicted ν to be

$$\begin{aligned} \Delta \nu_{\text{psr}} &= \Delta \dot{\nu}_{\text{on}} \Delta t_{\text{on},1} + \Delta \dot{\nu}_{\text{off}} \Delta t_{\text{off},1} + \Delta \dot{\nu}_{\text{on}} \Delta t_{\text{on},2} + \dots \\ &= \sum_{i=1}^N \Delta \dot{\nu}_i \Delta t_i. \end{aligned} \quad (9)$$

In light of this, it will be possible to detect the presence of a variable $\dot{\nu}$ in the timing residuals of a pulsar when the condition $\Delta \nu_{\text{psr}} \gg \Delta \nu_{\text{mod}}$ is satisfied (where $\Delta \nu_{\text{mod}}$ is the uncertainty in the model ν over a time span T). With the above in mind, we computed the expected $\Delta \nu_{\text{psr}}$ over the course of three subsequent emission phases (of total length T), assuming an average deviation in spin-down rate $|\Delta \dot{\nu}_{\text{av}}| = |\langle \dot{\nu}_{\text{obs}} - \dot{\nu}_{\text{pred}} \rangle|$, for a wide range of parameters (see Fig. 11). We note that, while these data do not precisely model $\Delta \nu_{\text{psr}}$, they do offer useful estimates that can be used to predict the detection limits on $\Delta \dot{\nu}$ in pulsars.

Assuming PSR B0823+26 exhibits a maximum modulation timescale $\Delta t \sim 1$ d (hence $T \sim 3$ d), and $|\Delta \dot{\nu}_{\text{av}}| \sim 9.7 \times 10^{-17} \text{ s}^{-2}$, we would expect $\Delta \nu_{\text{psr}} \sim 2.5 \times 10^{-11} \text{ Hz}$. This is approximately 2000 times smaller than $\Delta \nu_{\text{mod}}$ from our timing measurements ($\sim 5 \times 10^{-8} \text{ Hz}$), which can clearly explain why we do not find direct evidence for multiple $\dot{\nu}$ values. Comparing this with PSR B1931+24, we find that $\Delta \nu_{\text{psr}} / \Delta \nu_{\text{mod}} \sim 3$, for $|\Delta \dot{\nu}_{\text{av}}| = 8.8 \times 10^{-16} \text{ s}^{-2}$ and $\langle T \rangle \sim 40$ d, does result in significant detection of a variable $\dot{\nu}$. This indicates that our method of calculation for $\Delta \nu_{\text{psr}}$ is robust, and that it is not large enough in PSR B0823+26 to facilitate the detection of a variable $\dot{\nu}$.

Moreover, considering that the maximum null duration resolved in PSR B0823+26 (during the continuous observing runs) is about 5 h, it is likely that $\Delta \nu_{\text{psr}}$ is overestimated by a factor of ~ 5 . Therefore, it is not unsurprising that $\Delta \nu_{\text{psr}}$ is not significant enough to require the incorporation of another $\dot{\nu}$ in the timing model. In light of this result, it is extremely likely that $\Delta \dot{\nu}$ will not be discernible in a significant proportion of nulling pulsars.

¹⁰ In fact, we propose that deviation from a simple spin-down model could in principle be used to infer the magnetic inclination angle of a source in an independent fashion.

With the above in mind, it is interesting to determine the typical properties of a pulsar which can facilitate the detection of $\Delta\dot{\nu}$. If we assume a typical pulsar has $\dot{\nu}_{\text{av}} = -4.46 \times 10^{-15} \text{ s}^{-2}$, $|\Delta\dot{\nu}_{\text{av}}| \sim 4.5 \times 10^{-16} \text{ s}^{-2}$ (i.e. $\sim 10\%$ of $\dot{\nu}_{\text{av}}$) and a detection threshold $\Delta\nu_{\text{psr}}/\Delta\nu_{\text{mod}} \sim 5$, then we should expect to detect spin-down rate variation in pulsars which exhibit $T \gtrsim 26 \text{ d}$ and have a timing precision $\Delta\nu_{\text{mod}} \sim 10^{-9} \text{ Hz}$ or better. The majority of mode-changing and nulling pulsars, however, do not exhibit such long modulation timescales (e.g. Wang et al. 2007; Keane et al. 2010; Burke-Spolaor & Bailes 2010; Burke-Spolaor et al. 2011; Keane et al. 2011). Accordingly, we argue that it will be extremely difficult to determine whether $\dot{\nu}$ switching is a global phenomenon in these sources, especially those with very short modulation timescales (i.e. \lesssim hours). Clearly, more observations of similar objects are required before a consensus is reached on their common properties, and how PSR B0823+26 fits into their framework.

6 CONCLUSIONS

We have found evidence to suggest that PSR B0823+26 exhibits a broad distribution of nulling timescales i.e. \lesssim minutes up to several hours or more. Although longer duration nulls (\sim day) have been observed in our data, we cannot rule out the presence of short-term variations \lesssim minutes in the radio-off phases which we are insensitive to; radio emission flickering, which was observed in the continuous observing runs as ‘pre-ignition’ radio pulses, could have occurred during times of low observation cadence and, hence, been missed. As such, long (\sim hours) single-pulse observations of this source are required to confirm its overall nulling fraction, emission intermittency timescales and, therefore, its periodicity; that is if the source does not exhibit random emission fluctuations. These data should also provide further information as to why nulling (a.k.a. intermittent) pulsars might undergo emission flickering before they assume a stable magnetospheric state.

A simulation tool was developed to reproduce the timing behaviour observed in intermittent radio pulsars. This tool provides evidence for an upper limit of approximately 6% on the variation in the spin-down rate of PSR B0823+26. However, we cannot rule out a scenario where the pulsar retains a constant, single $\dot{\nu}$. Nevertheless, the low limit on $\Delta\dot{\nu}_{\text{max}}$, compared with that observed in PSR B1931+24 ($\sim 50\%$; Kramer et al. 2006), suggests the importance of small changes to the global charge distribution of a pulsar magnetosphere, which might easily perturb the production or detectability of radio emission. With this in mind, PSR B0823+26 could provide a link between conventional nulling and more extreme pulsar intermittency, due to the long timescale radio emission modulation and small change in $\dot{\nu}$ between emission phases.

Despite the somewhat unique emission geometry of PSR B0823+26 which facilitates its detection as an inter-pulse pulsar, no morphological clue has been provided to explain its intermittent behaviour. This is primarily due to a dearth of studies which attempt to correlate pulsar emission geometry with pulse intensity modulation, as well as the ordinary location of the object in the $P - \dot{P}$ diagram which, ultimately, make it extremely difficult to discern the general properties (e.g. P , \dot{P} and α) of the source from the bulk of the normal pulsar population. It is interesting to note, however, that the object undergoes intermittent behaviour without the need for large changes in spin-down rate, contrary to that predicted by Li et al. (2012a) ($\dot{\nu}_{\text{on}}/\dot{\nu}_{\text{off}} \sim 120\%$ for $\alpha \sim 90^\circ$). In this context, it may only be pulsars which exhibit long modulation timescales (\gtrsim days to weeks) that experience such

large changes in $\dot{\nu}$. Ultimately, further (multi-frequency) study of PSR B0823+26, and other objects like it, should reveal significant information about the nature of normal nulling pulsars, RRATs and longer-term intermittent pulsars. This, in turn, should offer the possibility to determine how all these objects are related (if they are), what their typical characteristics are and what mechanism is governing their irregular behaviour.

7 ACKNOWLEDGEMENTS

We thank A. A. Zijlstra, A. Shukurov, D. J. Champion and M. D. Gray for useful discussions which have contributed to this work. We also acknowledge C. Jordan, and the several telescope operators at Jodrell Bank, who have overseen the many hours of observations used in this paper.

REFERENCES

- Addison P. S., 2002, *The Illustrated Wavelet Transform Handbook: Introductory Theory and Applications in Science, Engineering, Medicine and Finance*. IoP, Bristol and Philadelphia
- Backer D. C., 1970, *Nature*, 228, 42
- Backer D. C., Boriakoff V., Manchester R. N., 1973, *Nature*, 243, 77
- Bartel N., Morris D., Sieber W., Hankins T. H., 1982, *ApJ*, 258, 776
- Becker W., Weisskopf M. C., Tennant A. F., Jessner A., Dyks J., Harding A. K., Zhang S. N., 2004, *ApJ*, 615, 908
- Bedding T. R., Zijlstra A. A., Jones A., Foster G., 1998, *MNRAS*, 301, 1073
- Biggs J. D., 1992, in Hankins T. H., Rankin J. M., Gil J. A., eds, *The Magnetospheric Structure and Emission Mechanisms of Radio Pulsars*, IAU Colloquium 128 Meridional Compression of Radio Pulsar Beams. Pedagogical University Press, Zielona Góra, Poland, pp 22–25
- Burke-Spolaor S., Bailes M., 2010, *MNRAS*, 402, 855
- Burke-Spolaor S., Bailes M., Johnston S., Bates S. D., Bhat N. D. R., Burgay M., D’Amico N., Jameson A., Keith M. J., Kramer M., Levin L., Milia S., Possenti A., Stappers B., van Straten W., 2011, *MNRAS*, 416, 2465
- Camilo F., Ransom S. M., Chatterjee S., Johnston S., Demorest P., 2012, *ApJ*, 746, 63
- Contopoulos I., 2005, *A&A*, 442, 579
- Cordes J. M., Shannon R. M., 2008, *ApJ*, 682, 1152
- Craft H. D., Lovelace R. V. E., Sutton J. M., 1968
- Deich W. T. S., Cordes J. M., Hankins T. H., Rankin J. M., 1986, *ApJ*, 300, 540
- Esamdin A., Lyne A. G., Graham-Smith F., Kramer M., Manchester R. N., Wu X., 2005, *MNRAS*, 356, 59
- Everett J. E., Weisberg J. M., 2001, *ApJ*, 553, 341
- Foster G., 1996, *Astron. J.*, 112, 1709
- Geppert U., Rheinhardt M., Gil J., 2003, *A&A*, 412, L33
- Gwinn C. R., Taylor J. H., Weisberg J. M., Rawley L. A., 1986, *AJ*, 91, 338
- Hesse K. H., Wielebinski R., 1974, *A&A*, 31, 409
- Hobbs G., Lyne A. G., Kramer M., 2010, *MNRAS*, 402, 1027
- Hobbs G. B., Edwards R. T., Manchester R. N., 2006, *MNRAS*, 369, 655
- Jones D. I., 2012, *MNRAS*, 420, 2325
- Keane E. F., 2010, PhD thesis, The University of Manchester

- Keane E. F., Kramer M., Lyne A. G., Stappers B. W., McLaughlin M. A., 2011, MNRAS, 415, 3065
- Keane E. F., Ludovici D. A., Eatough R. P., Kramer M., Lyne A. G., McLaughlin M. A., Stappers B. W., 2010, MNRAS, 401, 1057
- Kramer M., Lyne A. G., O'Brien J. T., Jordan C. A., Lorimer D. R., 2006, Science, 312, 549
- Li J., Spitkovsky A., Tchekhovskoy A., 2012a, ArXiv e-prints
- Li J., Spitkovsky A., Tchekhovskoy A., 2012b, ApJ, 746, 60
- Li X.-H., Lu F.-J., Li Z., 2008, ApJ, 682, 1166
- Lorimer D. R., 1994, PhD thesis, The University of Manchester
- Lorimer D. R., Kramer M., 2005, Handbook of Pulsar Astronomy. Cambridge University Press
- Lorimer D. R., Yates J. A., Lyne A. G., Gould D. M., 1995, MNRAS, 273, 411
- Lyne A., Hobbs G., Kramer M., Stairs I., Stappers B., 2010, Science, 329, 408
- Lyne A. G., Ashworth M., 1983, MNRAS, 204, 519
- Maciesiak K., Gil J., Ribeiro V. A. R. M., 2011, MNRAS, 414, 1314
- Manchester R. N., Taylor J. H., 1977, Pulsars. Freeman, San Francisco
- McLaughlin M. A., Lyne A. G., Lorimer D. R., Kramer M., Faulkner A. J., Manchester R. N., Cordes J. M., Camilo F., Possenti A., Stairs I. H., Hobbs G., D'Amico N., Burgay M., O'Brien J. T., 2006, Nature, 439, 817
- Politis, D.N. Romano, J.P. Wolf, M. 1999, Subsampling. Springer-Verlag, New York
- Rankin J. M., 1986, ApJ, 301, 901
- Rankin J. M., Wright G. A. E., 2007, MNRAS, 379, 507
- Rathnasree N., Rankin J. M., 1995, ApJ, 452, 814
- Rheinhardt M., Konenkov D., Geppert U., 2004, A&A, 420, 631
- Ritchings R. T., 1976, MNRAS, 176, 249
- Rosen R., McLaughlin M. A., Thompson S. E., 2011, ApJL, 728, L19
- Scargle J. D., 1982, ApJ, 263, 835
- Shao, J. Tu, D. 1995, The Jackknife and the Bootstrap. Springer-Verlag, New York
- Templeton M., 2004, Journal of the American Association of Variable Star Observers (JAAVSO), 32, 41
- Templeton M. R., Mattei J. A., Willson L. A., , 2005, Secular Evolution in Mira Variable Pulsations
- Tepedelenlioğlu E., Ögelman H., 2005, ApJL, 630, L57
- Timokhin A. N., 2010, MNRAS, pp L133+
- Urpin V., Gil J., 2004, A&A, 415, 305
- van Leeuwen A. G. J., Kouwenhoven M. L. A., Ramachandran R., Rankin J. M., Stappers B. W., 2002, A&A, 387, 169
- Wang N., Manchester R. N., Johnston S., 2007, MNRAS, 377, 1383
- Wang N., Manchester R. N., Johnston S., Rickett B., Zhang J., Yusup A., Chen M., 2005, MNRAS, 358, 270
- Zhang B., Qiao G. J., Lin W. P., Han J. L., 1997, ApJ, 478, 313
- Zoubir, A.M. Iskander, D.R. 2004, Bootstrap Techniques for Signal Processing. Cambridge University Press, Cambridge